


Diaphragm Involvement in Duchenne Muscular Dystrophy (DMD): An MRI Study

Francesca Pennati, PhD,^{1,2*}  Filippo Arrigoni, MD,² Antonella LoMauro, MSc,¹ Sandra Gandossini, MD,² Annamaria Russo, MD,² Maria G. D'Angelo, MD,² and Andrea Aliverti, PhD¹

Background: Duchenne muscular dystrophy (DMD) is characterized by progressive weakness and wasting of skeletal, cardiac, and respiratory muscles, with consequent cardiopulmonary failure as the main cause of death. Reliable outcome measures able to demonstrate specific trends over disease progression are essential.

Purpose: To investigate MRI as a noninvasive imaging modality to assess diaphragm impairment in DMD. In particular, we sought to correlate MRI measurement of diaphragm structure and function with pulmonary function tests and with the abdominal volumes (V_{AB}) measured by optoelectronic plethysmography, being an index of the action of the diaphragm.

Study Type: Cross-sectional study.

Population: Twenty-six DMD patients (17.9 ± 6.2 years) and 12 age-matched controls (17.8 ± 5.9 years).

Field Strength/Sequence: 3-Point gradient echo Dixon sequence at 3T.

Assessment: Images were acquired in breath-hold at full-expiration (EXP) and full-inspiration (INSP). INSP and EXP lung volumes were segmented and the diaphragm surface was reconstructed as the bottom surface of the left and the right lung. The inspiratory and the expiratory diaphragm surfaces were aligned by a nonrigid iterative closest point algorithm. On MRI we measured: 1) craniocaudal diaphragmatic excursion; 2) diaphragm fatty infiltration.

Statistical Tests: Three-parameter sigmoid regression, one-way analysis of variance (ANOVA), Spearman's correlation.

Results: In patients, diaphragm excursion decreased with age ($r^2 = 0.68$, $P < 0.0001$) and fat fraction increased ($r^2 = 0.51$, $P = 0.0002$). In healthy subjects, diaphragm excursion and fat fraction had no relationship with age. Diaphragm excursion decreased with decreasing FEV₁ %pred ($r = 0.78$, $P < 0.0001$) and FVC %pred ($r = 0.76$, $P < 0.0001$) and correlated with V_{AB} ($r = 0.60$, $P = 0.0002$). Fatty infiltration increased with decreasing FEV₁ %pred ($r = -0.88$, $P < 0.0001$) and FVC %pred ($r = -0.88$, $P < 0.0001$).

Data Conclusion: The progressive structural and functional diaphragm impairment is highly related to pulmonary function tests and to V_{AB} . The results suggest that MRI might represent a new and noninvasive tool for the functional and structural assessment of the diaphragm.

Level of Evidence: 2

Technical Efficacy Stage: 5

J. MAGN. RESON. IMAGING 2019.

DUCHENNE MUSCULAR DYSTROPHY (DMD) is an X-linked myopathy, in which the mutation of the gene coding for the dystrophin protein leads to progressive weakness and wasting of skeletal, cardiac, and respiratory muscles, with consequent cardiopulmonary failure as the main cause of death.¹ Treatments such as noninvasive mechanical ventilation (NIMV) and cough assistance machines allow for prolongation of life expectancy.² Measuring respiratory function is necessary

to assess and monitor respiratory capacity and to predict the need for artificial ventilation.^{3,4}

Spirometry is recognized as an essential tool for routine lung function evaluation in DMD and annual forced vital capacity (FVC) measurement is recommended, since FVC has prognostic value for survival and is a useful marker for treatment efficacy.⁵ The patient is asked to fully inhale, to reach total lung capacity, and then to exhale as forcefully as possible,

View this article online at wileyonlinelibrary.com. DOI: 10.1002/jmri.26864

Received May 14, 2019, Accepted for publication Jun 27, 2019.

*Address reprint requests to: F.P., Dipartimento di Elettronica, Informazione e Bioingegneria, Politecnico di Milano, P.zza L. da Vinci, 32, 20133 Milano, Italy. E-mail: francesca.pennati@polimi.it

The last two authors contributed equally to this work.

From the ¹The Dipartimento di Elettronica, Informazione e Bioingegneria, Politecnico di Milano, Italy; and ²Scientific Institute, IRCCS E. Medea, Bosisio Parini, Italy

to reach residual volume, with FVC being the forced, maximal expiratory volume. Nevertheless, pulmonary function tests (PFTs) measure the overall lung function as the result of the interaction of all respiratory muscles and do not distinguish the specific involvement of individual respiratory muscles.

With the progression of DMD, the diaphragm becomes progressively weak^{6,7} and its fatigue index increases,⁸ its action reduces to the point that paradoxical cephalic movement may occur, while its thickness increases, indicating pseudohypertrophy due to infiltration of connective tissue and fat deposition.^{9,10} It is therefore important to study the diaphragm in these patients, as its weakness is the main cause of hypoventilation,⁷ nocturnal desaturation,¹¹ and inefficient cough.¹² Specific diaphragmatic outcome measures are therefore needed to objectively evaluate the progression of the disease to try to determinate the proper time to start specific intervention.

Optoelectronic plethysmography (OEP) is a motion capture system that, using infrared TV cameras, passive reflective markers, and dedicated geometrical models, provides, without the use of a mouthpiece, accurate measurements of the thoracoabdominal contributions to tidal volume.¹³ The abdominal contribution to tidal volume is considered a good surrogate of the action of the diaphragm and current studies on subjects with DMD have shown that the reduction of diaphragm contribution to tidal volume is a good marker of disease progression.⁷

Magnetic resonance imaging (MRI) is being increasingly used in neuromuscular diseases to assess muscle size and structure, and to study the progressive fatty infiltration of the lower and upper limbs muscles.^{14–16} Static MRI studies on respiratory muscles' involvement are reported in Pompe disease, grading muscular atrophy on axial and coronal images¹⁷ and measuring in a sagittal view the craniocaudal and the anteroposterior thoracic movement.¹⁸ One 3D MRI study in Pompe disease reported by Mogalle et al measures differences in craniocaudal, anteroposterior, and left–right lung diameters after manual lung segmentation.¹⁹ Recently, cine-MRI has been applied in DMD to study the dynamic motion of the chest wall and of the diaphragm on sagittal images in patients younger than 15 years old.^{20,21} Nevertheless, the temporal resolution required for a dynamic acquisition leads to low spatial resolution and challenging image analysis.^{20,21} Furthermore, in these previous studies diaphragm kinematics was investigated by following the temporal profile of the lung cross-section and not in 3D, thus not allowing to track modifications across different regions of the diaphragm.

The aim of the present study was to examine whether static MRI provides adjunctive measures of the diaphragm impairment in DMD patients. In particular, we aimed to investigate quantitative MRI endpoints of diaphragm mobility and fat infiltration in relation to age and to clinical measures of respiratory function in DMD patients and healthy subjects.

Materials and Methods

Study Subjects

This study was approved by the local Ethics Committee and written informed consent was obtained from each subject or legal guardian.

Patients with a defined diagnosis of DMD, ranging in age from 6–32 years, followed at the "E. Medea Scientific Institute" were consecutively enrolled in the study between September 2016 and September 2017. Diagnosis of DMD was based on physical examination, elevated creatine kinase, and genetic and biopsy confirmation of dystrophin mutation or absence, according to established international diagnostic criteria.²² Exclusion criteria were: claustrophobia, cognitive deficits, all-day dependence on noninvasive mechanical ventilation, inability to stay still in the scanner, and perform a 10-second breath-hold. According to steroid therapy, patients were classified as naïve (never treated or treated for <1 year), past (not under treatment, but previously treated for >1 year), or current (under treatment or treated within 1 year from the enrollment).

Age-matched healthy male controls were recruited among relatives of the researchers and students of the laboratory who volunteered to take part to the study, excluding those subjects with respiratory diseases.

DMD patients and controls were subdivided into two groups according to age: ≤ 15 and > 15 years old. This subdivision of our patients is related to the published literature data of DMD, reporting a lower abdominal contribution to tidal volume, and therefore lower diaphragmatic contribution to breathing, after 15 years of age.⁷

Spirometry

Spirometry was performed in DMD patients on the same day of MRI. Measurements of forced-expiratory volume in 1 second (FEV1), forced vital capacity (FVC), forced expiratory flow at 25–75% of FVC (FEF 25–75), forced expiratory flow at 50% of FVC (FEF 50), and peak expiratory flow (PEF) were performed in a seated position. Data were reported both as absolute and expressed as percentage of the predicted values, computed according to a prediction equation calculated on healthy subjects of similar characteristics (body height, age, sex, and sometimes race and weight).²³

Optoelectronic Plethysmography

The breathing pattern was measured in a supine position by optoelectronic plethysmography (OEP-System; BTS, Milan, Italy) using a geometrical model of 52 markers,¹³ both in patients and in controls on the same day of MRI. After a short period of adaptation to the recording conditions, total and compartmental volumes were measured during 5 minutes of quiet breathing and inspiratory capacity maneuver (IC) from functional residual capacity to total lung capacity. The following parameters were calculated breath-by-breath during spontaneous tidal breathing: tidal volume (V_T), respiratory rate (RR), minute ventilation, rapid and shallow breathing index (RSBI; calculated as RR/V_T), and ribcage and abdominal tidal volumes (ΔV_{RC} and ΔV_{AB} , respectively, expressed both in liters and as percentage contribution to V_T). The following parameters were calculated during the IC maneuver: maximal inspiratory total volume (IC_{cw}), ribcage and abdominal volumes (ΔV_{RC_IC} and ΔV_{AB_IC} , respectively, expressed both in liters and as percentage contribution to IC_{cw}).

MR Image Acquisition

Patients and controls were scanned with a 3T MR system (Philips Achieva dStream scanner, Philips Medical Systems, Best, The Netherlands). The imaging protocol included multiple 3-point gradient echo Dixon sequences (repetition time / echo time [TR/TE] = 2.9/2.3 msec, flip angle 10°, slice thickness 4.4 mm, in-plane resolution 1.09 × 1.09 mm × mm) acquired at suspended full end-expiration (EXP) (approximately residual volume [RV]), and suspended full end-inspiration (INSP) (approximately total lung capacity [TLC]). The field of view was adjusted both in inspiration and expiration depending on subject anatomy, to both cover the entire lungs and minimize the acquisition time. Images were acquired in the coronal plane; during 10–12 seconds of breath-hold. To reduce the scan time a SENSE acceleration factor of 2 was used.

Before the imaging session, patients were instructed to sustain TLC and RV volumes during the scan. Images were checked by the radiologist and reacquired during the same imaging session if not satisfactory. All patients were experienced in performing respiratory maneuvers because they were used to spirometric tests during their follow-up. No sedation or contrast material was used. Overall acquisition time per subject, including positioning, was ~15 minutes.

MR Image Processing and Measurements

Image processing and quantitative analysis were performed by custom software developed in MatLab (MathWorks, Natick, MA).

MEASUREMENT OF DIAPHRAGM EXCURSION. The image acquisition, processing, and quantitative analysis is summarized in Fig. 1. The steps are the following:

1. Image acquisition at full-expiration and full-inspiration (Fig. 1a). The in-phase images were used to estimate the diaphragm excursion.

2. Lung segmentation (Fig. 1b). The method automatically selected the optimal threshold that separated low-density tissue (ie, lung and air surrounding the patient) from the surrounding chest wall, based on Otsu's algorithm. Trachea and main bronchi were reconstructed and subtracted from the original images using a 3D confidence connected region-growing algorithm.²⁴
3. Diaphragm reconstruction. The bottom surfaces of the left and the right lungs were automatically extracted by identifying the most inferior voxels of the segmented lungs, which were characterized by a negative curvature of the lower lung contours on coronal and sagittal slices. Delaunay triangulation was used to generate the triangular meshes of the left and right hemidiaphragm.
4. Surface registration. The inspiratory and the expiratory meshes were first rigidly aligned by matching their centroids. Then a nonrigid iterative closest point algorithm (NCIP)²⁵ was used to non-rigidly register the inspiratory and the expiratory diaphragm surfaces. NCIP extends the iterative closest point algorithm by assuming local affine transformation for each vertex, and iteratively minimizes the distance between source and target meshes with adjustable stiffness constraint.
5. Apicocaudal diaphragm excursion. The vertical component of the deformation field represented the apicocaudal excursion of the diaphragm. The median value of the apicocaudal excursion of the overall diaphragm surface was computed and reported as "global" excursion. Regions of interest (ROIs, about 100-mm²-area circles) were manually selected in the dome area and near the posterior costal margin to evaluate regional differences in the diaphragm motion.

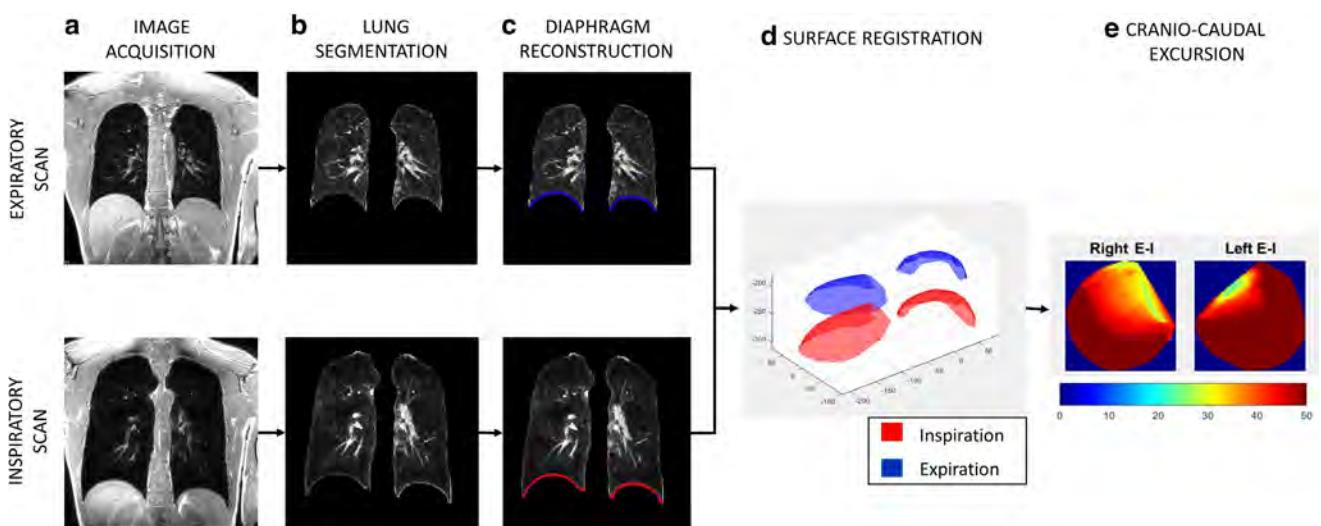


FIGURE 1: Image processing steps. (a) MR images were acquired in breath-hold at full-expiration and full inspiration and (b) automatically segmented on the basis of Otsu's method. (c) The bottom surfaces of the left and the right lungs were extracted from the segmented lungs and the Delaunay triangulation was used to generate the triangular meshes of the left and right hemidiaphragm. (d) The surface reconstructed in expiration (blue) is registered on the surface reconstructed in inspiration (red). (e) The craniocaudal excursion is obtained as the vertical component of the vector field.

MEASUREMENT OF DIAPHRAGM FAT INFILTRATION.

The amount of fat was determined on the inspiratory images with the three-point Dixon technique,²⁶ which allows the separation of MR signal intensity into the individual contribution of fat and water in each voxel. The scanner software uses an IDEAL based algorithm^{27,28} to compute water signal (SIwater) and fat signal (Sifat) images, while taking into account field inhomogeneity, eddy currents, and T₂* effect. Fat and water images were loaded in the Medical Image Processing, Analysis, and Visualization application (MIPAV v. 7.2.0; <http://mipav.cit.nih.gov>) and quantitative fat infiltration (percentage fat) was computed as: Sifat/(Sifat+SIwater). 3D ROIs were manually traced over the costal and crural parts of the diaphragm by two observers (F.P. with 8 years experience in pulmonary imaging and F.A. with 13 years experience in MRI). Particular attention in ROIs tracing was paid to avoid partial volume effects with the surrounding structures.

Fat infiltration was also measured in paraspinal muscles at the level of the aortic arch and of the top diaphragm for comparison. The median values are reported.

Statistical Analysis

Statistical analysis was performed using SigmaStat v. 11.0 (Systat Software, San Jose, CA).

The relationships between age and both diaphragm excursion and fat infiltration were modeled by fitting the data to a three-parameter sigmoid curve, as we expected that MRI parameters will plateau to normal values in younger patients and to maximal diaphragm impairment in older patients, approaching a floor of -0 mm of diaphragm excursion and a plateau of 100% of fat fraction. The fitting equation for the sigmoid curve is:

$$y = \frac{a}{1 + \exp^{-b(AGE - AGE_0)}}$$

where y is the excursion (mm) or fat fraction (%) over age (years). Coefficient a (mm or %) is the upper horizontal asymptote, AGE₀ (years) is the age-to-half peak corresponding also to the age at the point of highest sigmoid curve slope, coefficient b (years⁻¹) is proportional to the slope of the curve in AGE₀, ie, slope (AGE₀) = a · b/4(mm/year). The coefficients of determination (r²) were computed for all the regression analysis.

One-way analysis of variance (ANOVA) was applied to separately compare diaphragm excursion (global, central, and dome), diaphragm fat fraction, and paraspinal fat fraction across age (<15 vs. >15) and disease state (healthy vs. DMD). In cases in which the equal variance test and/or the normality test fail, non-parametric Kruskal–Wallis ANOVA on ranks was applied. Post-hoc tests were based on Holm–Sidak and Dunn methods, respectively for parametric and nonparametric ANOVA tests.

Spearman’s correlation coefficients (r values) were calculated between MRI biomarkers of diaphragm impairment, spirometry, and OEP in healthy and DMD patients.

For all the statistical analysis, significance was set to P < 0.05.

Results

In total, 26 patients (mean age 17.9 ± 6.2 years; range 8–32 years) and 12 age-matched healthy subjects were enrolled in the study. Clinical data and spirometry are reported in Table 1 for DMD patients. All subjects successfully completed the MRI protocol. Due to logistic reasons, in two patients and one healthy volunteer OEP was not performed.

Diaphragm Excursion With Age

Figure 2 reports the relationship between global and regional diaphragm excursion and age in DMD patients (Fig. 2, left column) and controls (Fig. 2, central column). Diaphragm excursion (DE) decreased with age with the following sigmoid relations:

$$DE_{global} = \frac{49.7}{1 + \exp^{0.17(AGE - 14.6)}}$$

$$DE_{costal} = \frac{57.1}{1 + \exp^{0.20(AGE - 15.2)}}$$

TABLE 1. Patient Data, Reported as Median (25th–75th Percentile)

Age (years)	17 (14–22)	
FEV ₁ (l)	1.5 (0.8–1.8)	
FEV ₁ (%pred)	54 (20–85)	
FVC (l)	1.6 (1.0–2.4)	
FVC (%pred)	55 (22–81)	
FEF 25–75 (l)	1.9 (1.0–2.5)	
FEF 25–75 (%pred)	40 (21–57)	
FEF 50 (l)	2.1 (1.4–3.0)	
FEF 50 (%pred)	58 (34–75)	
PEF (l/sec)	3.1 (2.1–4.2)	
PEF (%pred)	49 (25–78)	
Steroid	Past (n)	7
	Current (n)	11
	Naïve (n)	8
Ambulation	Yes (n)	6
	No (n)	20
LVEF (%)	58 (50–60)	

FEV₁, forced expiratory volume in 1 second; FVC, forced vital capacity; FEF25-75 = forced expiratory flow at 25–75% of FVC, FEF50 = forced expiratory flow at 50% of FVC; PEF, peak expiratory flow; LVEF, left ventricular ejection fraction.

$$DE_{dome} = \frac{49.5}{1 + \exp^{0.15(AGE-13.5)}}$$

The r^2 were respectively 0.51 ($P = 0.0002$), 0.57 ($P < 0.0001$), and 0.51 ($P = 0.0003$). In healthy volunteers, global, costal, and dome DEs were higher than in DMD patients ($P < 0.001$), with no relationship with age (respectively $P = 0.55$). In subjects younger than 15 years old, DE was lower in patients compared with controls, in the costal and dome regions but not globally (Fig. 2, right column).

DE was lower in patients older than 15 years than in controls, both globally and regionally in the costal and dome regions (Fig. 2, right column).

In Fig. 3 the diaphragm surfaces (Fig. 3a) reconstructed in expiration (blue) and inspiration (red) and the corresponding apicocaudal excursion maps (Fig. 3b) are reported in three representative patients 9 (Fig. 3, left), 14 (Fig. 3, center), and 26 (Fig. 3, right) years old. With increasing age, the inspiratory and the expiratory diaphragm surfaces become closer and closer, with the 26-year-old patient showing a paradoxical motion,

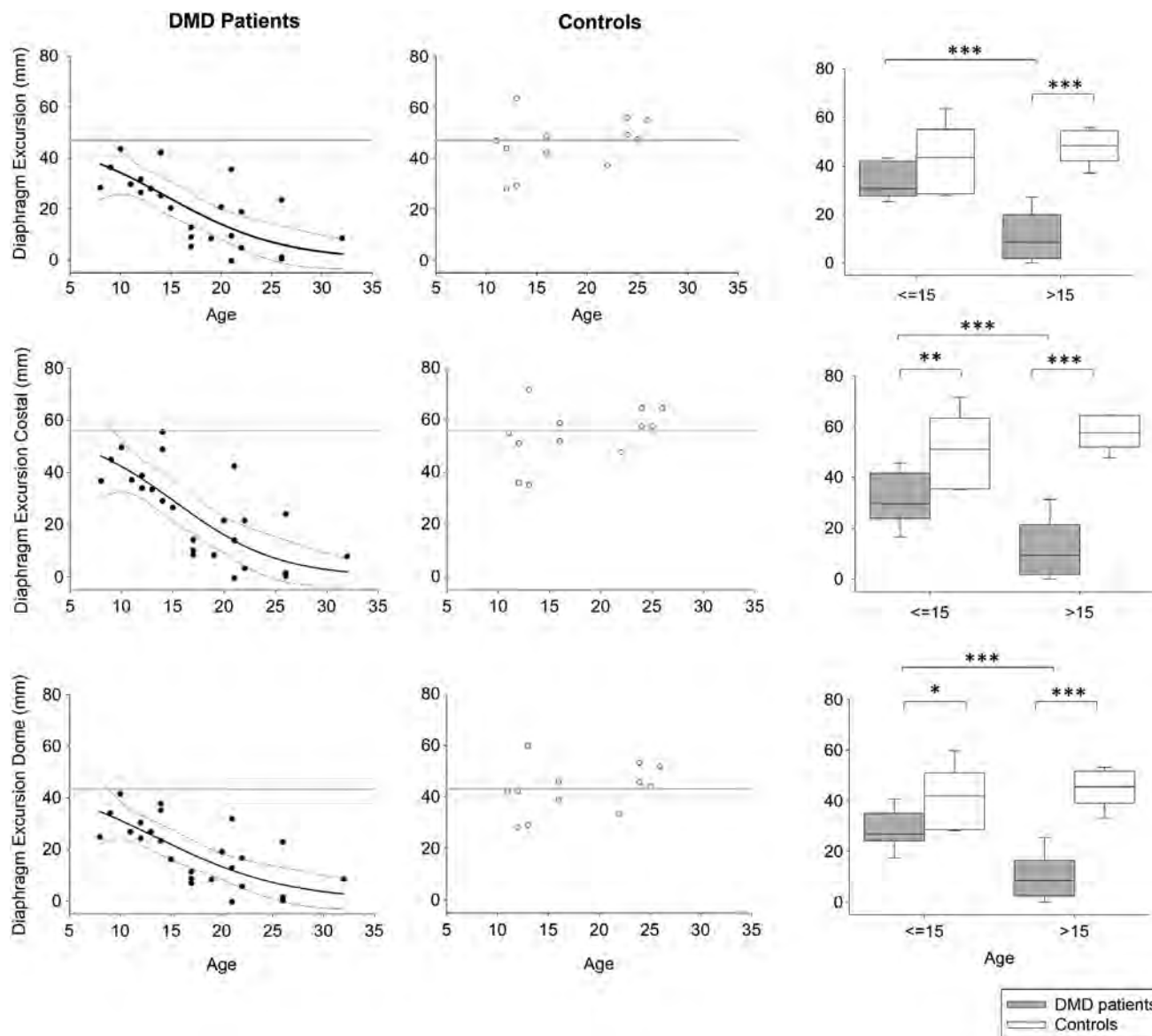


FIGURE 2: Correlation between global (top row), costal (central row), dome (bottom row) diaphragm excursion (DE) and age in patients with DMD (left column) and healthy controls (central column). In patients with DMD, DE decreases with age following a sigmoidal relationship: $r^2 = 0.51$ ($P = 0.0002$, overall data); $r^2 = 0.57$ ($P < 0.0001$, costal regions); $r^2 = 0.51$ ($P = 0.0003$, dome regions). In healthy controls, no relationship between DE and age is present. Left panels: regression curve (thick black line) and 95% confidence intervals (thin black lines) of DE data in DMD patients; median value (thick gray line), 25th and 75th percentiles (thin gray lines) of DE data in the control group. Central panels: median value (thick gray line), 25th and 75th percentiles (thin gray lines) of DE data in the control group. Right panels: Box-and-whisker plot representing the median (line within the box), the interquartile range (length of the box), the 90th and the 10th percentiles (whiskers above and below the box) of DE calculated in DMD patients (gray) and healthy controls (white) younger and older than 15 years. * $P < 0.05$; ** $P < 0.01$; *** $P < 0.001$.

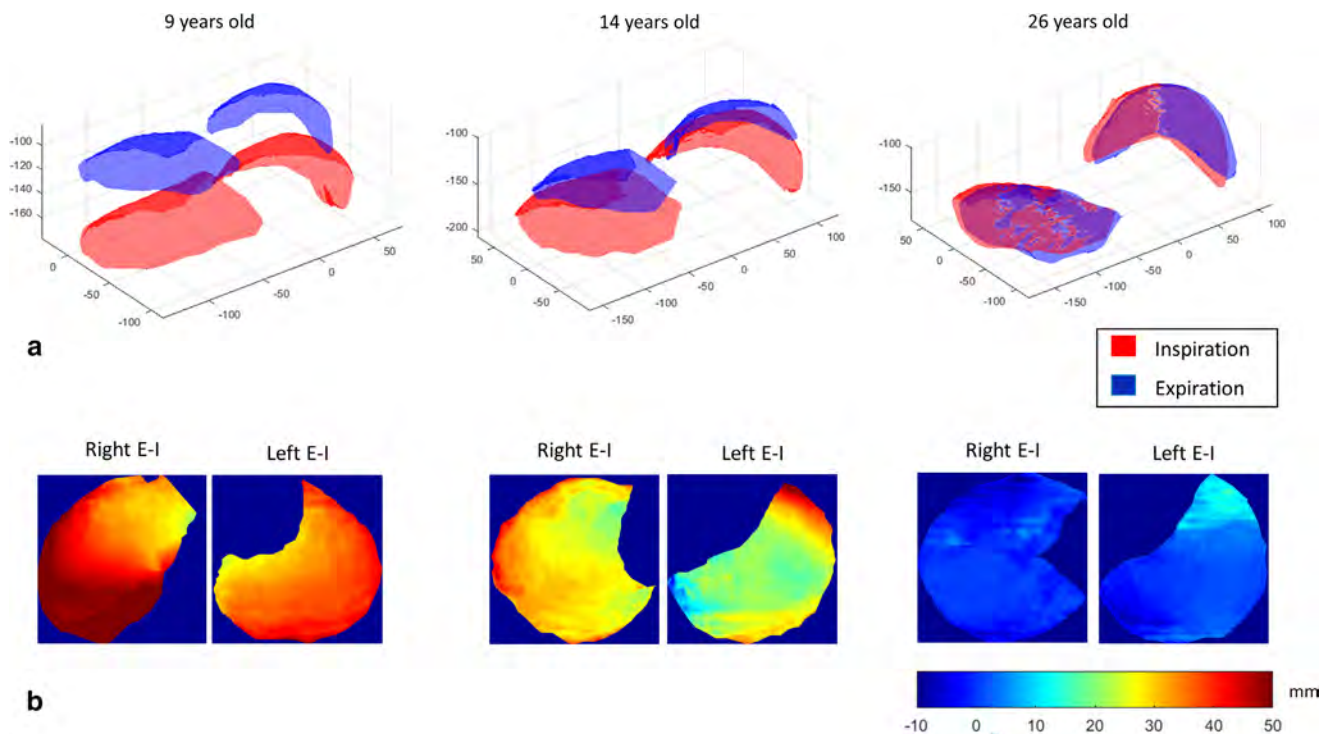


FIGURE 3: (a) Expiratory (blue) and inspiratory (red) diaphragm 3D surface reconstruction in three representative patients at 9 (left, FEV₁ = 127 %pred), 14 (central, FEV₁ = 50 %pred), and 26 (right, FEV₁ = 16 %pred) years old. (b) Corresponding maps of craniocaudal excursion. Color scale indicates the vertical excursion in mm.

with the diaphragm moving cranially from expiration to inspiration. The apicocaudal excursion map in the younger patient is mainly colored in red, corresponding to apicocaudal excursions of about 50 mm. Conversely, in the oldest patient, the excursion map is mainly colored in light blue, corresponding to an apicocaudal excursion below 10 mm, with some regions colored in dark blue, corresponding to negative values of excursion.

Diaphragm Fat Infiltration With Age

No significant differences were found between crural and costal fat infiltration ($P = 0.75$), thus the median value of the two regions is reported as a more robust measure of the fat infiltration of the overall diaphragm. Figure 4 shows the relationship between fat infiltration and age in the diaphragm (Fig. 4, top row) and in the paraspinal muscles (Fig. 4, bottom row) in DMD patients (Fig. 4, left column) and in healthy volunteers (Fig. 4, central column). In patients, diaphragm fat fraction increased with age with a sigmoidal relationship ($r^2 = 0.68$, $P < 0.0001$):

$$FF_{diaphragm}(\%) = \frac{80.9}{1 + \exp^{-0.17(AGE - 14.8)}}$$

In controls, median fat infiltration of the diaphragm was 26.1% (20.7–27.4%), lower than in DMD patients ($P < 0.001$), with no relationship with age ($P = 1.0$).

Fat fraction of the paraspinal muscles in patients increased with age with the relationship ($r^2 = 0.72$, $P < 0.0001$):

$$FF_{paraspinal}(\%) = \frac{93.7}{1 + \exp^{-0.25(AGE - 15.2)}}$$

In controls, median fat fraction of the paraspinal muscles was 10.9% (8.4–11.4%), lower than in DMD patients ($P < 0.001$), with no relationship with age ($P = 1.0$).

At the age of about 15 years, the increase in percent fat fraction was 3.4 per year and 5.8 per year, respectively, for the diaphragm and the paraspinal muscles.

In Fig. 5 the fat infiltration of the diaphragm is shown in three representative patients 9 (Fig. 5, left), 14 (Fig. 5, center), and 26 (Fig. 5, right) years old. In the fat fraction images, the diaphragm is mainly black in the younger patient, corresponding to a fat fraction of about 0%. Conversely, in the oldest patient the diaphragm is mainly light gray, corresponding to fat fraction over 80%.

Relationship Between MRI Parameters of Diaphragm Impairment, Spirometry, and OEP

Table 2 reports the Spearman’s coefficients (r) of correlations between MRI markers of diaphragm impairment in patients, ie, DE and fat infiltration, spirometry, and OEP.

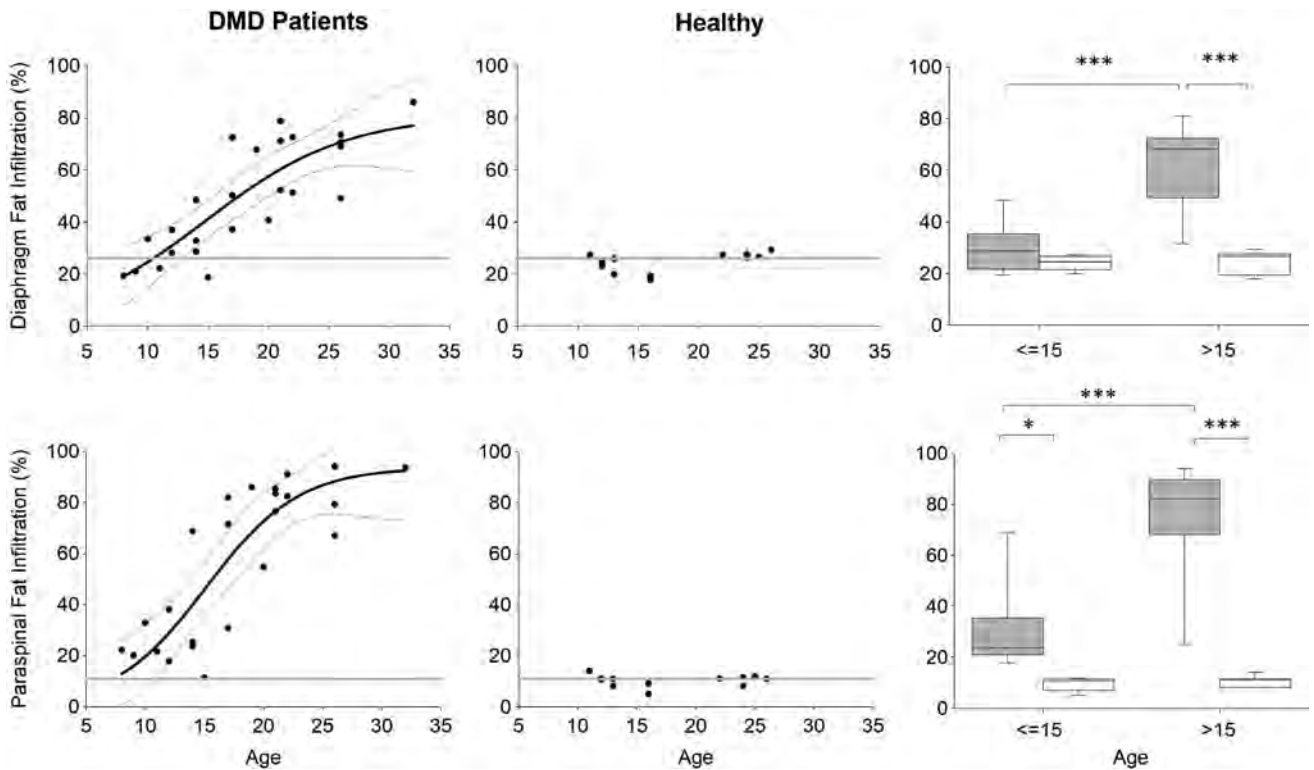


FIGURE 4: Correlation between diaphragm (top row), paraspinal muscles (bottom row) fat infiltration, and age in patients with DMD (left column) and healthy controls (central column). In patients, fat infiltration increases with age following a sigmoidal relationship: $r^2 = 0.68$ ($P < 0.0001$, diaphragm); $r^2 = 0.72$ ($P < 0.0001$, paraspinal muscle). In healthy controls, no relationship between fat infiltration and age is present. Left panels: regression curve (thick black line) and 95% confidence intervals (thin black lines) of fat fraction data in DMD patients; median value (thick gray line), 25th and 75th percentiles (thin gray lines) of fat fraction data in the control group. Central panels: median value (thick gray line), 25th and 75th percentiles (thin gray lines) of fat fraction data in the control group. Right panels: Box-and-whisker plot representing the median (line within the box), the interquartile range (length of the box), the 90th and the 10th percentiles (whiskers above and below the box) of fat fraction calculated in DMD patients (gray) and healthy controls (white) younger and older than 15 years. * $P < 0.05$; *** $P < 0.001$.

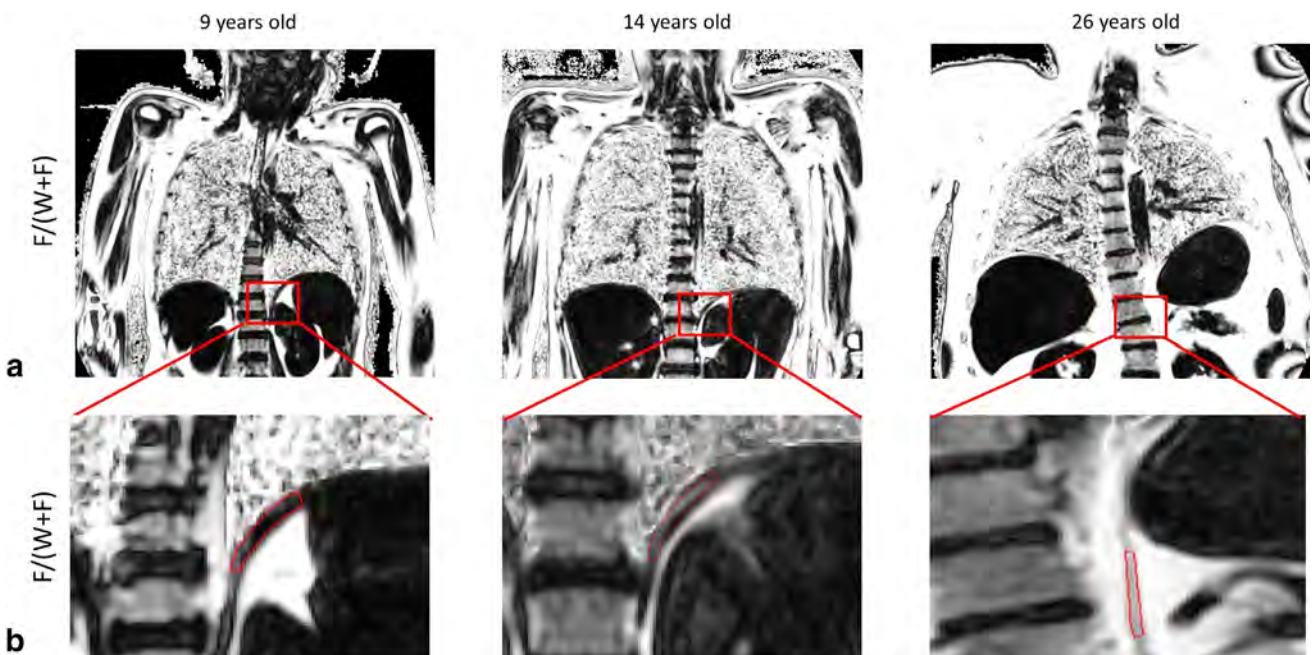


FIGURE 5: Fat infiltration of the diaphragm in three representative patients at 9 (left, FEV1 = 127 %pred), 14 (central, FEV1 = 50 % pred), and 26 (right, FEV1 = 16 %pred) years old. (a) Fat fraction map calculated as $F/(W+F)$ in %. (b) Magnification of the diaphragm. The region of interest is selected in red.

TABLE 2. Spearman' Correlation Coefficients (r) Between MRI Markers of Diaphragm Impairment (Global, Costal and Dome Apicocaudal Excursion, and Fat Infiltration), Spirometry and OEP Parameters

		Apicocaudal excursion	Apicocaudal excursion (costal)	Apicocaudal excursion (dome)	Diaphragm fat infiltration
SPIROMETRY	FEV1 (l)	0.69***	0.70***	0.67***	-0.69***
	FEV1 (%pred)	0.78***	0.80***	0.76***	-0.88***
	FVC (l)	0.58**	0.59**	0.56**	-0.60**
	FVC (%pred)	0.76***	0.79***	0.73***	-0.88***
	FEF25-75(l)	0.59**	0.61**	0.58**	-0.56**
	FEF25-75 (%pred)	0.62**	0.64***	0.61**	-0.63**
	FEF50(l)	0.51**	0.53**	0.50*	-0.51*
	FEF50 (%pred)	0.70***	0.72***	0.68***	-0.74***
	PEF (l/sec)	0.54**	0.53**	0.54**	-0.53**
	PEF (%pred)	0.79***	0.80***	0.78**	-0.89***
OEP	<i>Quiet breathing</i>				
	RSBi	-0.24	-0.21	-0.24	0.16
	RR	-0.15	-0.12	-0.14	0.07
	V _t	0.24	0.21	0.24	-0.23
	ΔV_{RC} (l)	-0.36*	-0.36*	-0.35*	0.17
	ΔV_{RC} (%)	-0.60***	-0.58***	-0.59***	0.28
	ΔV_{AB} (l)	0.66***	0.63***	0.66***	-0.37*
	ΔV_{AB} (%)	0.60***	0.59***	0.60***	-0.30
	<i>Inspiratory capacity</i>				
	IC _{CW} (l)	0.85***	0.83*** (P < 0.0001)	0.84***	-0.70***
	ΔV_{RC} (l)_IC	0.74***	0.72*** (P < 0.0001)	0.72***	-0.66***
	ΔV_{RC} (%)_IC	-0.37*	-0.36*	-0.38*	0.27
	ΔV_{AB} (l)_IC	0.71***	0.69***	0.71***	-0.59***
	ΔV_{AB} (%)_IC	0.36*	0.36*	0.38*	-0.26

Spirometry was performed in patients. OEP was performed both in healthy controls and patients.

FEV1 = forced-expiratory volume in 1 second; FVC = forced vital capacity; FEF25-75 = forced expiratory flow at 25-75% of FVC, FEF50 = forced expiratory flow at 50% of FVC; PEF = peak expiratory flow; V_t = tidal volume; RSBi = rapid and shallow breathing index; RR = respiratory rate; ΔV_{RC} (l) = rib cage volume variation expressed in liters; ΔV_{AB} (%) = rib cage volume variation expressed as percentage contribution to tidal volume; ΔV_{AB} (l) = abdominal volume variation expressed in liters; ΔV_{AB} (%) = abdominal volume variation expressed as percentage contribution to tidal volume.

*P < 0.05;

**P < 0.01;

***P < 0.001.

Total and regional apicocaudal excursions of the diaphragm positively correlated with all the spirometric values. Fat infiltration correlated negatively with all the spirometric values. The highest correlations were found between MRI markers and PEF %pred.

Total and regional apicocaudal excursion of the diaphragm positively correlated with abdominal volume variation and negatively correlated with rib cage volume variation. Fat infiltration negatively correlated with abdominal volume variation.

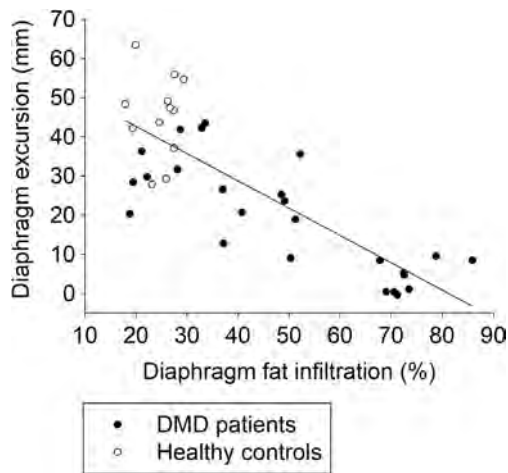


FIGURE 6: Linear relationship between diaphragm structure, ie, fat infiltration, and function, ie, apicocaudal excursion ($r^2 = 0.63$, $P < 0.0001$). White circles represent healthy volunteers; black circles DMD patients.

Structure–Function Relationship of the Diaphragm

Figure 6 shows the linear relationship between DE and fat infiltration, considering both healthy controls and DMD patients, with $r^2 = 0.66$ ($P < 0.0001$). Considering only DMD patients, a linear relationship exists between the two MRI parameters, with $r^2 = 0.63$ ($P < 0.0001$).

Discussion

The present cross-sectional study demonstrates that multi-volume MRI provides valuable quantitative measures of diaphragm impairment in patients with DMD. Diaphragm structure and function are highly related with age, with a sigmoidal relationship and respiratory function decline, as quantified by pulmonary function tests and OEP. With the development of new therapeutic and rehabilitative approaches for DMD, MRI may provide new noninvasive outcome measures to follow up the involvement of the respiratory muscles for use in clinical trials.

The first result of our study regards the vertical excursion of the diaphragm. We have shown that in DMD patients the maximal excursion decreases with age and is significantly different from controls in patients older than 15 years of age. When the costal and dome contribution to the vertical excursion are separately studied, significant differences between DMD and healthy subjects younger than 15 years can also be observed. Studying DE by 2D cine-MRI in a group of patients younger than 15 years old, Bishop et al²¹ reported differences in the right dome excursion between DMD and healthy subjects. These previous findings and the here-reported reduced dome and costal excursions across a larger age span demonstrate the ability of MRI to detect early signs of diaphragm weakness. Static and dynamic MRI can provide information regarding diaphragmatic motion^{29,30} and has been investigated in emphysema³¹ and in patients with

scoliosis.³² In neuromuscular disease, diaphragm kinematics has been described in Pompe disease in 2D by using static breath-hold MRI images^{18,33} and in 3D by acquiring dynamic MRI.¹⁹ The craniocaudal DE measured in absolute values on normal subjects varies across studies, due to different subject characteristics and different methods for diaphragm displacement's measure. The measurements obtained in the present study in controls are consistent with previously reported values, 4.6–9.0 cm,³³ 5.1–8.1 cm.¹⁹ With respect to these previous studies, we acquired static breath-hold MR images with a 3-point gradient echo Dixon sequence, in order to simultaneously quantify both DE and fat infiltration, thus to directly relate structure to function.

Second, the present study demonstrated that the fat fraction of the diaphragm progressed with age, and significantly differed from healthy patients older than 15 years old. Compared with paraspinal muscles, we observed a slower increase in the fat fraction of the diaphragm and a lower heterogeneity among patients. In the diaphragm, no MRI data on fat fraction have been previously reported. In patients, fat fraction increase per year in the quadriceps and hamstrings was about 5% between 5 and 23 years old³⁴ and 6–9% between 4 and 13 years old,³⁵ higher than the annual fat fraction increase of the diaphragm and of the paraspinal muscles that we have found in the present study. With respect to these previous findings, we proposed a sigmoidal equation to fit the fat fraction vs. age relationship, which could have influenced the computation of the annual increase of fat fraction. Nevertheless, as the age span of our patients was wider, ie, 8–32 years old, we preferred to use a phenomenological model to describe the fat fraction increase and the excursion decrease of the diaphragm with age. The proposed model is in accord with recent studies investigating the natural course of pulmonary function loss in DMD: at around 10–11 years of age, FVC %pred falls below the 80% predicted, which is considered the lower limit of normal, follows a quite linear decline, and approaches a floor of 20% of predicted from age 20 onwards.^{7,36}

Third, we found that the fat fraction and the functional ability of the diaphragm were strongly correlated. Prior studies have found high degrees of correlation between MRI measures of fat fraction of quickly degenerating proximal muscles and ambulatory function, measured using the 10-m walk/run, the climb four stairs, supine to stand, and 6-minute walk tests.^{15,37–39} With respect to these studies, we directly related the fat fraction increase of the diaphragm to its excursion function; thus, the structure–function relationship was investigated free from any compensatory mechanisms. Studies performed by using ultrasonography (US) showed a progressive diaphragm atrophy with age and reduced excursion.^{9,10} Laviola et al¹⁰ reported that diaphragmatic thickness was similar to the control group in DMD patients younger than 14 years old, but that it was significantly lower in patients

older than 14 years old. Our results confirmed the diaphragm remodeling, with increased fat fraction after 15 years old, and the reduced excursion in DMD patients.

Fourth, MRI markers of diaphragm impairment correlated with OEP measures and spirometry. During quiet breathing, the DE is positively related to the abdominal volume variation and inversely related to the rib cage expansion. As DE decreases, thus decreasing abdominal volume variation, ribcage volume variation increases. This result suggests that the ribcage muscles partially compensate the diaphragm impairment, by increasing ribcage volume variation, in order to retain tidal volume which, in fact, is not correlated with diaphragm impairment. Moreover, diaphragm fat infiltration correlated only with the abdominal volume variation, reinforcing the idea that the first functional biomarker of the diaphragm impairment is the reduction of abdominal volume during quiet breathing.⁷ On the contrary, when both MRI and OEP were performed during inspiratory capacity, the diaphragm impairment highly correlated with all the OEP parameters. During the maneuver, all the respiratory muscles have to maximally contract. The positive relationship between the MRI measures of diaphragm impairment and both the abdominal and the ribcage volume variation suggests that during a maximal contraction the ribcage muscles are ineffective to compensate the diaphragm. This is confirmed by the strong correlation between diaphragm impairment and spirometry, which is also performed during a maximal contraction. Contraindications to MRI such as metal implants, invasive ventilation, and claustrophobia make it impossible to scan certain patients. Nevertheless, different from OEP and spirometry, MRI is able to directly measure both diaphragm structure and function, thus providing new noninvasive and sensitive outcome measures that should be considered for longitudinal studies in DMD and for clinical trials.

Over dynamic MRI techniques, static MRI provides higher spatial resolution and reduced scan time, simplifying image analysis and allowing the use of automatic algorithms for 3D lung segmentation and diaphragm reconstruction. The diaphragm kinematics have been previously investigated in neuromuscular disease, by following the 2D temporal profile of the lung cross-section from a dynamic MRI acquisition^{20,21} or by measuring changes in lung dimensions between inspiration and expiration.^{18,33} The 3D representation of the diaphragm allows a more accurate and robust analysis, with the possibility of tracking and evaluating different regions. Moreover, the simultaneous quantification of DE and fat fraction provide shorter scan durations for patients who cannot stay in the scanner for a long time or cannot perform multiple deep-breath cycles.

The study has some limitations. First, it includes a small number of patients. Nevertheless, the age range is broad enough to study the progressive structural and functional impairment of the diaphragm during the course of the

disease. Although the age range explored is larger than that in previous studies, only two patients younger than 10 years old were examined. Since symptoms of DMD can begin at a few years old, it might be beneficial to perform a future study focusing on the age range 5–15 years old. Second, MR images are not spirometer-guided. To introduce quantitative multivolume MRI in clinical practice, the implementation of lung volume guidance with a spirometer is essential to standardize imaging.⁴⁰ Finally, diaphragm kinematics were investigated only along the vertical axis. In fact, in order to reduce the acquisition time and make the imaging session more comfortable for patients, we decided to adapt the field of view to the inspiratory and the expiratory lung volumes, thus changing the reference point of the image with lung volume. Future studies investigating the overall lung kinematic should be performed, but considering only younger patients, who are able to perform breath-holding at residual volume for a longer time.

In conclusion, this work provides an efficient method to extract quantitative measures of diaphragm structure and function in DMD from static MRI, which are strongly correlated with spirometry and OEP. Quantitative MRI of the diaphragm seems to be a promising endpoint for clinical trials evaluating the effect of newer treatments on the time to start ventilation in DMD.

Acknowledgments

Contract grant sponsor: Fondo DMD Amici di Emanuele Onlus.

The authors thank all patients and families for their collaboration and the medical personnel of the IRCCS "E. Medea" involved in the care and evaluation of the patients and data insertion (C. Pistininzi, E. Marchi, M. Grandi, V. Landoni).

References

- Hoffman EP, Brown RH, Kunkel LM. Dystrophin: The protein product of the Duchenne muscular dystrophy locus. *Cell* 1987;51:919–928.
- Finder JD, Birnkrant D, Carl J et al. Respiratory care of the patient with Duchenne muscular dystrophy. *Am J Respir Crit Care Med* 2004;170:456–465.
- Bushby RF, Finkel R, Birnkrant DJ, et al. Diagnosis and management of Duchenne muscular dystrophy. Part 1: Diagnosis, and pharmacological and psychosocial management. *Lancet Neurol* 2010;9:77–93.
- Bushby K, Finkel R, Birnkrant DJ, et al. Diagnosis and management of Duchenne muscular dystrophy. Part 2: Implementation of multidisciplinary care. *Lancet Neurol* 2010;9:177–189.
- Phillips MF, Quinlivan RCM, Edwards RHT, Calverley PMA. Changes in spirometry over time as a prognostic marker in patients with Duchenne muscular dystrophy. *Am J Respir Crit Care Med* 2002;164:2191–2194.
- Nicot F, Hart N, Forin V, et al. Respiratory muscle testing: A valuable tool for children with neuromuscular disorders. *Am J Respir Crit Care Med* 2006;174:67–74.

7. LoMauro A, Romei M, Gandossini S, et al. Evolution of respiratory function in Duchenne muscular dystrophy from childhood to adulthood. *Eur Respir J* 2018;51.
8. Matecki S, Topin N, Hayot M, et al. A standardized method for the evaluation of respiratory muscle endurance in patients with Duchenne muscular dystrophy. *Neuromuscul Disord* 2001;11:171–177.
9. De Bruin PF, Ueki J, Bush A, Khan Y, Watson A, Pride NB. Diaphragm thickness and inspiratory strength in patients with Duchenne muscular dystrophy. *Thorax* 1997;52:472–475.
10. Laviola M, Priori R, D'Angelo MG, Aliverti A. Assessment of diaphragmatic thickness by ultrasonography in Duchenne muscular dystrophy (DMD) patients. *PLoS One* 2018;13:e0200582.
11. Romei M, D'Angelo MG, Lomauro A, et al. Low abdominal contribution to breathing as daytime predictor of nocturnal desaturation in adolescents and young adults with Duchenne muscular dystrophy. *Respir Med* 2012;106:276–283.
12. LoMauro A, Romei M, D'Angelo MG, Aliverti A. Determinants of cough efficiency in Duchenne muscular dystrophy. *Pediatr Pulmonol* 2014;49:357–365.
13. Aliverti A, Dellacà R, Pelosi P, Chiumello D, Gattinoni L, Pedotti A. Compartmental analysis of breathing in the supine and prone positions by optoelectronic plethysmography. *Ann Biomed Eng* 2001;29:60–70.
14. Forbes SC, Willcocks RJ, Triplett WT, et al. Magnetic resonance imaging and spectroscopy assessment of lower extremity skeletal muscles in boys with Duchenne muscular dystrophy: A multicenter cross sectional study. *PLoS One* 2014;9:1–8.
15. Wokke BH, van den Bergen JC, Versluis MJ, et al. Quantitative MRI and strength measurements in the assessment of muscle quality in Duchenne muscular dystrophy. *Neuromuscul Disord* 2014;24:409–416.
16. Arrigoni F, De Luca A, Velardo D, et al. Multiparametric quantitative MRI assessment of thigh muscles in limb-girdle muscular dystrophy 2A and 2B. *Muscle Nerve* 2018 [Epub ahead of print].
17. Gaeta M, Barca E, Ruggeri P, et al. Late-onset Pompe disease (LOPD): Correlations between respiratory muscles CT and MRI features and pulmonary function. *Mol Genet Metab* 2013;110:290–296.
18. Gaeta M, Musumeci O, Mondello S, et al. Clinical and pathophysiological clues of respiratory dysfunction in late-onset Pompe disease: New insights from a comparative study by MRI and respiratory function assessment. *Neuromuscul Disord* 2015;25:852–858.
19. Mogalle K, Perez-Rovira A, Ciet P, et al. Quantification of diaphragm mechanics in Pompe disease using dynamic 3D MRI. *PLoS One* 2016;11:1–24.
20. Mankodi A, Kovacs W, Norato G, et al. Respiratory magnetic resonance imaging biomarkers in Duchenne muscular dystrophy. *Ann Clin Transl Neurol* 2017;4:655–662.
21. Bishop CA, Ricotti V, Sinclair CDJ, et al. Semi-automated analysis of diaphragmatic motion with dynamic magnetic resonance imaging in healthy controls and non-ambulant subjects with Duchenne Muscular Dystrophy. *Front Neurol* 2018;9:1–12.
22. Birnkrant DJ, Bushby K, Bann CM, et al. Diagnosis and management of Duchenne muscular dystrophy. Part 1: Diagnosis, and neuromuscular, rehabilitation, endocrine, and gastrointestinal and nutritional management. *Lancet Neurol* 2018;17:251–267.
23. Quanjer PH, Tammeling GJ, Cotes JE et al. Lung volumes and forced ventilatory flows. Report Working Party. Standardization of Lung Function Tests, European Community for Steel and Coal. Official Statement of the European Respiratory Society. *Eur Respir J* 1993;6 (Suppl.16):5–40.
24. Pennati F, Quirk JD, Yablonskiy DA, Castro M, Aliverti A, Woods JC. Assessment of regional lung function with multivolume 1 H MR imaging in health and obstructive lung disease: Comparison with 3 He MR imaging. *Radiology* 2014;273:580–590.
25. Amberg B, Romdhani S, Vetter T. Optimal step nonrigid ICP algorithms for surface registration. In: *Proc IEEE Comput Soc Conf Comput Vis Pattern Recognit*; 2007.
26. Glover GH, Schneider E. Three-point Dixon technique for true water/fat decomposition with B0 inhomogeneity correction. *Magn Reson Med* 1991;18:371–383.
27. Reeder SB, Pineda AR, Wen Z, et al. Iterative decomposition of water and fat with echo asymmetry and least-squares estimation (IDEAL): Application with fast spin-echo imaging. *Magn Reson Med* 2005;54:636–644.
28. Yu H, Shimakawa A, McKenzie CA, Brodsky E, Brittain JH, Reeder SB. Multiecho water-fat separation and simultaneous R* 2 estimation with multifrequency fat spectrum modeling. *Magn Reson Med* 2008;60:1122–1134.
29. Gauthier AP, Verbanck S, Estenne M, Segebarth C, Macklem PT, Paiva M. Three-dimensional reconstruction of the in vivo human diaphragm shape at different lung volumes. *J Appl Physiol* 1994;76:495–506.
30. Gierada DS, Curtin JJ, Erickson SJ, Prost RW, Strandt JA, Goodman LR. Diaphragmatic motion: Fast gradient-recalled-echo MR imaging in healthy subjects. *Radiology* 2014;194:879–884.
31. Iwasawa T, Kagei S, Gotoh T, et al. Magnetic resonance analysis of abnormal diaphragmatic motion in patients with emphysema. *Eur Respir J* 2002;19:225–231.
32. Chu WCW, Li AM, Ng BKW, et al. Dynamic magnetic resonance imaging in assessing lung volumes, chest wall, and diaphragm motions in adolescent idiopathic scoliosis versus normal controls. *Spine* 2006;31:2243–2249.
33. Wens SCA, Ciet P, Perez-Rovira A, et al. Lung MRI and impairment of diaphragmatic function in Pompe disease. *BMC Pulm Med* 2015;15:54.
34. Fischmann A, Hafner P, Gloor M, et al. Quantitative MRI and loss of free ambulation in Duchenne muscular dystrophy. *J Neurol* 2013;260:969–974.
35. Wren TAL, Bluml S, Tseng-Ong L, Gilsanz V. Three-point technique of fat quantification of muscle tissue as a marker of disease progression in Duchenne muscular dystrophy: Preliminary study. *AJR Am J Roentgenol* 2008;190:8–12.
36. Mayer OH, Finkel RS, Rummey C, et al. Characterization of pulmonary function in Duchenne muscular dystrophy. *Pediatr Pulmonol* 2015;50:487–494.
37. Gaeta M, Messina S, Mileto A, et al. Muscle fat-fraction and mapping in Duchenne muscular dystrophy: Evaluation of disease distribution and correlation with clinical assessments preliminary experience. *Skeletal Radiol* 2012;41:955–961.
38. Mankodi A, Bishop CA, Auh S, Newbould RD, Fischbeck KH, Janiczek RL. Quantifying disease activity in fatty-infiltrated skeletal muscle by IDEAL-CPMG in Duchenne muscular dystrophy. *Neuromuscul Disord* 2016;26:650–658.
39. Barnard AM, Willcocks RJ, Finanger EL, et al. Skeletal muscle magnetic resonance biomarkers correlate with function and sentinel events in Duchenne muscular dystrophy. *PLoS One* 2018;13:1–15.
40. Salamon E, Lever S, Kuo W, Ciet P, Tiddens HAWM. Spirometer guided chest imaging in children: It is worth the effort! *Pediatr Pulmonol* 2017;52:48–56.